https://doi.org/10.5194/egusphere-2026-3426
Preprint. Discussion started: 29 June 2026

Slope stability modelling in Karongi district, Western Rwanda

Sylvain Barayagwiza[1,★], Catherine A. Meriaux[1,★], and Alberto Armigliato[2,★]

[1]East African Institute for Fundamental Research/University of Rwanda, Kigali, Rwanda
[2]Dipartimento di Fisica e Astronomia "Augusto Righi",Alma Mater Studiorum – Università di Bologna,Viale Berti Pichat 8, Bologna, 40127, Italy
★These authors contributed equally to this work.

Correspondence: Sylvain Barayagwiza (barayagwizasylvain@gmail.com) and Catherine A. Meriaux (cmeriaux@eaifr.org).

Abstract. The Karongi District in Western Rwanda is frequently subject to landslides. To date, however, physics-based slope stability assessments remain pending. In this study, we apply a three-dimensional Limit Equilibrium Method (LEM) using Scoops3D software to compute Factor of Safety (FOS) distributions in Karongi District. The model evaluates the effects of the pore-pressure ratio (ru) and horizontal pseudo-static seismic coefficient (k_{eq}) on slope stability. Results identify critical thresholds at $ru \sim 0.10$ and $k_{eq} = 0.075$, beyond which unstable areas expand rapidly. When combined to pore pressure and at low pore pressure $ru \leq 0.10$, seismic loading can significantly amplify slope instability. Model validation using historical landslide inventories shows 80% spatial agreement between simulated unstable areas ($FOS < 1$) and observed landslides in two scenarios: (1) $ru = 0.18$ and $k_{eq} = 0.10$; and (2) $ru = 0.35$ and $k_{eq} = 0.03$. Although applied to the Karongi district, the methodology presented in this study can be used to assess the relative importance of pore pressure and seismic forcing in slope stability in a seismically active region prone to landslides.

1 Introduction

In several parts of the world landslides represent a significant threat to human lives, infrastructure, environment and socio-economic activities (Nwazelibe et al., 2023; Cruden and Varnes, 1996). The origin of landslides is complex, resulting from interactions between geological, meteorological, seismic, and anthropogenic factors. Understanding these interactions presents a challenge for the development of reliable landslide predictive models and early warning systems, particularly in low-capacity regions that are highly vulnerable to landslide impacts (Nwazelibe et al., 2023; Schuster and Highland, 2004). Along the Kivu rift (south-western branch of the East African Rift System), landslides are among the most destructive natural hazards due to steep-slope topography, seismicity, periods of intense rainfall, deforestation, and improper land use (Depicker et al., 2021b; Svalova et al., 2019). Like other parts of the Kivu Rift, Western Rwanda experiences frequent landslides during rainy seasons, when prolonged and intense rainfalls occur (Byiringiro et al., 2024). Most landslides in Rwanda are shallow, translational slides or debris flows (Byiringiro et al., 2024).

Several studies have recently been conducted in an effort to map landslide susceptibility in Rwanda at national, provincial, and district levels, recognizing that most landslides occurred during the last days of the rainfall season (Byiringiro et al., 2024; Niyibizi et al., 2025). These studies, mainly relying on field survey mapping, historical records, satellite images and aerial

https://doi.org/10.5194/egusphere-2026-3426
Preprint. Discussion started: 29 June 2026

photos interpretation (Nwazelibe et al., 2023; Malyse and Aboubakar, 2025), have highlighted the critical role of continuous water infiltration within the soil in slope instability. The western, southern and northern provinces of Rwanda are highly prone to landslides, the central part of western Rwanda (Karongi district), being the region most affected (Byiringiro et al., 2024; Nsengiyumva et al., 2018). More recently, Niyibizi et al. (2025) have conducted field work and laboratory soil tests along the road of Muhanga-Rutsiro-Karongi, specifically at the site named PK49 in Bigugu Village of Rutsiro district near the Rubengera Sector of Karongi district. Soil type was identified to be predominantly silty, with small amount of clay and some fine sand. The major interest of that study lies in the fact that it is one of the few to have characterized the physical parameters of the soil, a key element for slope stability and landslide modeling. The long rainfall period was also pointed out as an initiating trigger for slope failures through pore-pressure buildup within the slope materials.

Despite the advances that have been made, both in understanding the causal factors of landslides and identifying mitigation measures to be taken in Western Rwanda, no physics-based numerical model has been used yet. This study constitutes the first step in this direction by applying a slope stability modeling based on the Limit Equilibrium Method to calculate the Factor of Safety (FOS) for slope stability analysis in the Karongi district. Although the effects of rainfall on landslides are known, physical models describing the relationship between rainfall and pore-pressure remain to be developed (Ngaboyigihugu et al., 2025). They are also highly dependent on groundwater configuration and soil drainage, which are not always characterized, especially at a district scale. Under this constraint, we adopt a uniform pore-pressure ratio parameter in the models as the proxy for rainfall, and evaluate the effect of seismic loading on slope stability.

In this study, we first describe the study area of Karongi district in section 2. Section 3 presents the methodology. Section 4 illustrates the results, and section 5 discusses the results with the analysis of slope instability distribution, identifying the critical threshold pore-pressure ratio and horizontal pseudo-static acceleration coefficient, and compares the modeled results with historical landslide databases.

2 Study area

Karongi district is located in Western Rwanda, along the East African Rift (EAR; Figure 1). This district has an altitude ranging from 1460 to 2500 m above sea level (Figure 2a) with an average slope angle of no less than 30° as shown on Figure 2b. Its area covers 993 km^2 with a population density of 482 inhabitants per km^2, based on the fifth Rwanda population and housing census, 2022 (NISR, 2023). Rwanda experiences two rainy seasons each year: the first extends from March to May, while the second extends from September to December, with annual rainfall ranging from 1200 to 2200 mm. The spatial distribution of 1336 shallow landslides in Western Rwanda over the period 2000-2019 provided by Depicker et al. (2021a) (their supplementary material) is shown in Figure 1. It includes an exceptional cluster of more than 700 landslides during a single night (6–7 May 2018) over an area of 100 km^2 (Lat: 2.13°S-2.19°S; Long: 29.35°E-29.43°E) during extreme weather conditions (Byiringiro et al., 2024). According to Byiringiro et al. (2024), landslides in the Karongi district range from 50 m^2 to 68,000 m^2, with a shallow depth range of 0.5-2 m, leading to potential failure volumes comprised between 25 m^3 to 1.36×10^5 m^3, therefore in the range of small and medium landslides.

https://doi.org/10.5194/egusphere-2026-3426
Preprint. Discussion started: 29 June 2026

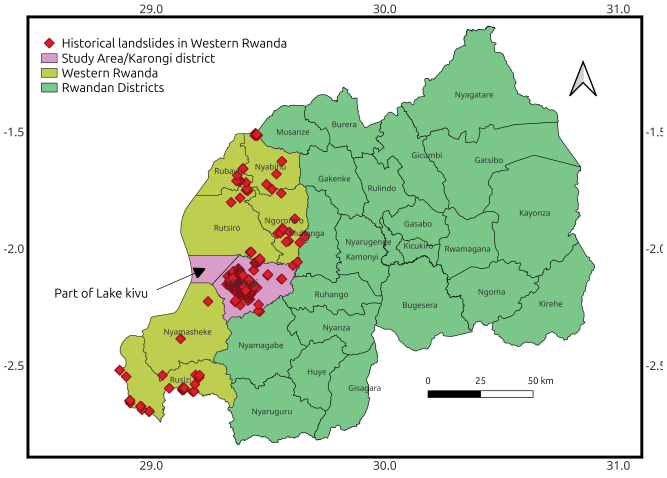

Figure 1. Map of Rwanda. The study area (Karongi district) is shown in pink; historical landslides in western Rwanda over the period 2000-2019 from Depicker et al. (2021a) are indicated as red diamonds

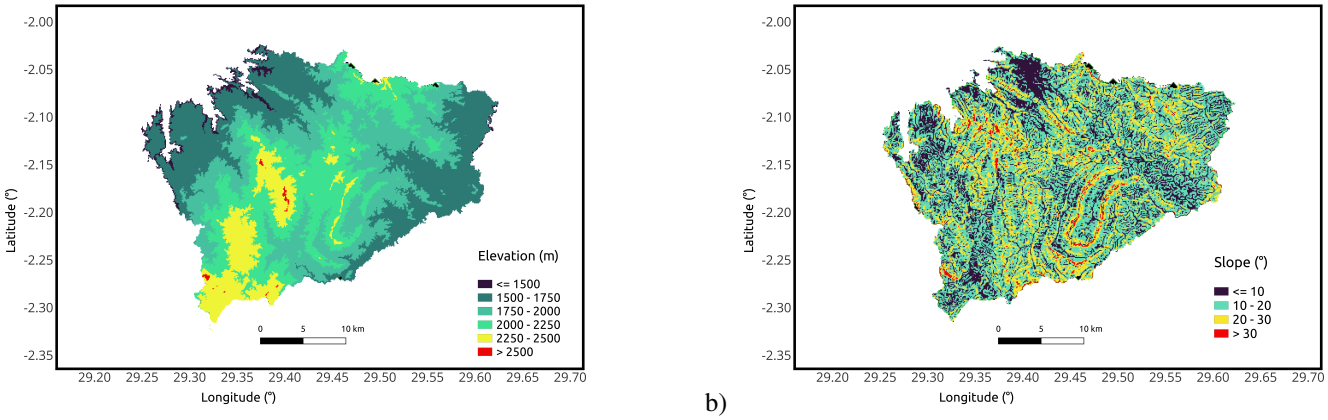

a) b)

Figure 2. a). Topographic map and b) slope map of the Karongi district. Both are derived from the 10 m resolution Digital Elevation Model (DEM) provided by Water and Sanitation Corporation (WASAC) in collaboration with Rwanda National Land Authority (NLA) (see Section 3.2.1)

Being along the western branch of the East African Rift, the district belongs to an active seismic region, as shown in Figure 3. Four events with magnitude greater than 5 (see Table 1) will later be used to calibrate the intensity of seismic loading.

https://doi.org/10.5194/egusphere-2026-3426
Preprint. Discussion started: 29 June 2026

Table 1. Selected Earthquakes (https://earthquake.usgs.gov/) used to calculate Horizontal Pseudo-acceleration coefficient, k_{eq} distribution presented on Figure 4.

Date	Latitude (°)	Longitude (°)	Depth (km)	Magnitude (Mw)
2002-10-24T06:08:37.980Z	-1.884	29.00	11	6.2
2008-02-03T07:34:12.180Z	-2.296	28.91	10	5.9
2015-08-07T01:25:02.540Z	-2.141	28.90	11	5.8
2003-03-20T06:15:20.580Z	-2.418	29.56	10	5.2

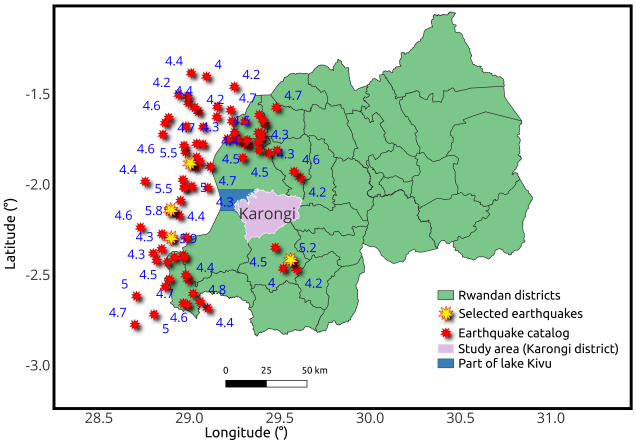

Figure 3. Selected Earthquake locations around the study area from https://earthquake.usgs.gov/earthquakes/search/. The earthquake catalog spans the period 2002-2025 and covers the magnitude interval 4.0 - 6.2 (the blue numbers in the figure)

3 Methodology

3.1 Computation of Factor of Safety (FOS)

In this paper, we use the open source software, Scoops3D (Reid et al., 2015) for slope stability simulations applying the Limit Equilibrium Method (LEM) -typically Bishop's simplified method- to compute the factor of safety, FOS. The FOS is defined as the ratio of shear strength to the shear stress as shown in Equation 1.

$$FOS = \frac{\text{Resisting force (shear strength)}}{\text{Driving force (shear stress)}} = \frac{S}{T}, \tag{1}$$

where S is the average shear resistance (strength) along the failure surface, and T is the shear stress required to maintain limit equilibrium. Based on the definition, a slope is considered stable if $FOS > 1$ and unstable if $FOS < 1$. The shear strength S of the soil along a potential slip surface is given by the Coulomb-Terzaghi failure criterion (Bishop, 1955; Bishop and

https://doi.org/10.5194/egusphere-2026-3426
Preprint. Discussion started: 29 June 2026

Morgenstern, 1960):

$$S = c + (N - u)\tan\phi, \tag{2}$$

where ϕ is the angle of internal friction, c is the cohesion, N is the normal stress and u is the pore-water pressure. On the other hand, the driving shear stress T is given by:

$$T = W\sin\alpha \tag{3}$$

where W is the normal force acting on each column of a potential failure mass and α is the local slope angle. The pore-water pressure u, which represents the hydraulic pressure acting on the soil skeleton due to groundwater,is given by:

$$u = h\gamma_w, \tag{4}$$

where h is the pressure head and γ_w is the unit weight of water (Bishop and Morgenstern, 1960). The pore water pressure ratio ru is then expressed as (Bishop and Morgenstern, 1960):

$$ru = \frac{u}{\int \gamma z dz} = \frac{u}{W/A_h}, \tag{5}$$

where γ is the unit weight of the overlying material and A_h is the horizontal area. Pore-water pressure ratio, ru, varies from 0 to 1, the latter value referring to a liquefied state where the pore-water pressure contributes to the vertical stress (Iverson, 2000; Osawa et al., 2023; Mousavi and Ghayoomi, 2020). $ru = 0.5$ corresponds to saturated conditions.

In the presence of seismic activity, the seismic load contributes to the shear stress T and is introduced in the form of a dimensionless horizontal pseudo-acceleration coefficient (k_{eq}) representing the ratio between the maximum ground acceleration and the gravitational acceleration, g. The local pseudo-acceleration coefficient is calibrated as a function of earthquake magnitude and epicentral distance.

To calculate FOS using Limit Equilibrium Method, Scoops3D divides the failure mass into vertical columns and computes their stability by calculating the balance of forces and torques on each column by assuming that the potential failure mass is a rigid body undergoing no internal deformation (Bishop and Morgenstern, 1960; Bishop, 1955; Reid et al., 2015).

Limit Equilibrium Method is a powerful tool for slope stability analysis due to its capability to physically visualize and calculate the force equilibrium on the slope at the point of failure and easy consideration of different parameters including soil properties, groundwater configuration, and seismic forcing.

3.2 Inputs for the computation

3.2.1 Digital Elevation Model (DEM)

This study uses a 10-m resolution Digital Elevation Model (DEM) providing information on local slopes (α) in the Karongi district. The resolution of the DEM selected here ensures a proper balance between computational efficiency and a level of

https://doi.org/10.5194/egusphere-2026-3426
Preprint. Discussion started: 29 June 2026

detail necessary for capturing topographic features characterizing that area. The DEM was provided by Water and Sanitation Corporation (WASAC) in collaboration with Rwanda National Land Authority (NLA)(https://geohub.data.undp.org/data/00d5add9be37e465398b081683c3ec03).

3.2.2 Soil properties in Karongi district

The soil types in Karongi district are dominated by Acrisols and Cambisols. These soils are predominantly silty, with small amount of clay and some fine sand (Byiringiro et al., 2024; Niyibizi et al., 2025), which potentially hold more water contributing to pore water pressure (Reid et al., 2015; Bishop and Morgenstern, 1960). This paper adopts the average geotechnical properties summarized in Table 2, as they were measured by Niyibizi et al. (2025) in Bigugu village of Rutsiro district, a site very close to Karongi district. These geotechnical parameters include the cohesion ranging from 3.2 to 4.22 kPa, the angle of internal friction ranging from 24.7 to 27.1° and the unit weight ranging from 16.2 to 16.5 kN/m^3.

Table 2. Assumed soil properties in Karongi district following measurements by Niyibizi et al. (2025).

Soil Properties	Values
Cohesion (c)	3.7 kPa
Angle of Internal friction (ϕ)	26°
Unit Weight (γ)	16.4 kN/m^3

3.2.3 Calibration of ground acceleration, k_{eq}

Ground acceleration due to an earthquake is typically represented as the combined result of a source, a propagation and a site effect term, plus uncertainty. Classical tools to estimate different intensity measures, the peak ground acceleration (PGA) being one of the most widely used, are the ground motion prediction equations (GMPE), also referred to as attenuation relationships. A large number of GMPE exist (see e.g. the compendium by Tuluka (2007)), tailored to different geographical, geomorphological, tectonic areas. Very few of them are conceived specifically for the East African Rift area: an example is provided by the regressions proposed by Tuluka (2007) for strong ground motion in the Kivu Province, Western Rift Valley of Africa, which we use here to calibrate end-member values of k_{eq} in the Karongi district based on :

$$k_{eq} = \frac{1.42 \exp(1.43M) R^{-a}}{g}, \tag{6}$$

where M is earthquake magnitude, R is the epicentral distance measured in km, a=1.1 when $M = 5$, a=1.2 when $M = 5.5-6.5$ and g is acceleration of gravity expressed in Gal ($g = 981$ Gal). Earthquake magnitudes in the region are typically of the order 4-5 and less frequently 6 (see Table 1 and Figure 3), whereas epicentral distances may vary between 20 km and 40 km, and even less in the extreme northeast and southwest as shown by Panelli et al. (2024) (their figure 3d). Assuming earthquakes of

https://doi.org/10.5194/egusphere-2026-3426
Preprint. Discussion started: 29 June 2026

magnitude 5 with the upper epicentral distance of 40 km, equation 6 provides $k_{eq} = 0.032$. When using the four earthquake events (see Table 1) with M $\geq$ 5 near to the study area, Figure 4 shows the spatial distribution of the resulting calculated horizontal pseudo-acceleration coefficients indicating that k_{eq} varies from 0.03 to 0.13.

On the other hand, such estimates appear to be conservative when compared to the Global Earthquake Model (GEM) Seismic Hazard Map (Panelli et al., 2024), providing the Peak Ground Acceleration (PGA) in terms of fraction of the acceleration of gravity, with a 10% probability of being exceeded in 50 years, computed for reference rock conditions (shear wave velocity, V_{s30} of 760-800 m/s). The GEM Seismic Hazard Map, resulting from a logic-tree approach involving different GMPE (see Chowdhury and Flentje (2011) for more details), provides values for k_{eq} in the range 0.13-0.35. This study will therefore consider the range of 0.03-0.35 for values of the pseudo-acceleration coefficient k_{eq}.

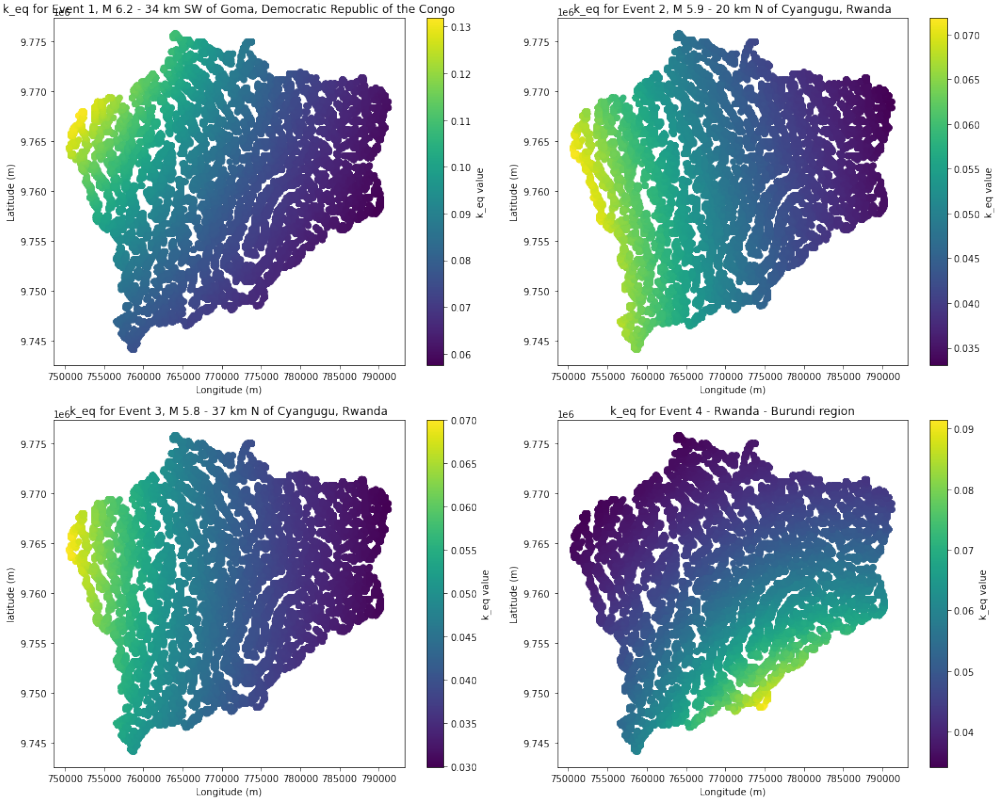

Figure 4. Horizontal Pseudo-acceleration coefficient, k_{eq} distribution in the study area for the four selected earthquakes listed in Table 1. Note that the colour scale is different in each plot

3.3 Simulation setup

To compute slope stability, we assume a homogeneous and uniform domain with one soil layer over the Karongi district. We therefore ignore the spatial variability of the soil types and depths. This simplification is justified by the lack of data available

https://doi.org/10.5194/egusphere-2026-3426
Preprint. Discussion started: 29 June 2026

at the scale of the district. Similarly, the pore-pressure ratio and seismic forcing are applied uniformly over the whole district. Scoops3D is bound to examine the safety factor relative to given potential failure volumes or areas. Here we chose as a criterion potential failure volumes on the order of 10^7 to 10^8 m^3. Such a chosen range of potential failure volumes is greater than the estimated landslide volumes by Byiringiro et al. (2024) in the Karongi district (min 25m^3 - max 10^5 m^3). However, analyzing the FOS over the entire district area for such small to medium landslide sizes would not only require DEMs of very high resolutions and small search radius increments of the spherical trial surfaces but also to divide the study area in multiple sub-domains to ensure both accurate solutions and computationally effective time and memory requirements. On the other hand, examining the safety factor for medium to large potential failure volumes highlights the most vulnerable areas in the district. Given this choice of potential failure volumes, we preprocessed the 10 m DEM in QGIS to convert it to a format readable by Scoops3D and modified its resolution to 100 m. Appendix A shows that using the 100 m DEM can provide comparable safety factors to those of the 10 m DEM for the given potential failure volume. Full details of the parameters adopted to run the simulations are given in the appendix.

Ground water effects are expressed as a proxy by means of systematic variation of the pore water pressure ratio ru due to the absence of other specific data such as piezometric and 3D pressure heads (Mousavi and Ghayoomi, 2020; Reid et al., 2015) in the study area. This approach does not account for rainfall infiltration, or spatial and temporal characteristics of rainfall. Thus, the values attributed to ru represent general hydrological conditions rather than in situ specific conditions. We note that the use of ru prevents taking into account negative pore-pressures. We note that the model does neither predict the deformation phase nor the movement that takes place after slopes fail. This model also assumes the potential failure surface to be a spherical shape undergoing rotational slip (Reid et al., 2015). It does not take into account planar, translational, or other complex geometries commonly known for shallow landslides or debris flow observed in western Rwanda. The approach of horizontal pseudo acceleration coefficient also ignores dynamic amplification and duration effects of seismic loading on slope stability. Despite these limitations, the adopted model remains appropriate, as it is widely used for slope stability assessment (Byiringiro et al., 2024; Niyibizi et al., 2025).

4 Results

This section discusses the results of three-dimensional slope stability analyses carried out under different conditions of pore water pressure ru and/or seismic loading k_{eq}.

4.1 Baseline slope stability under dry conditions ($ru = 0.0$) and no seismic loading ($k_{eq} = 0.0$)

Figure 5 shows the calculated initial slope stability map, obtained under dry conditions ($ru = 0.0$) and without seismic loading ($k_{eq} = 0.0$). It is used as a reference in evaluating the influence of pore water pressure and seismic loading on slope instability. Under these conditions, Karongi district shows FOS values greater than 1, representing moderate to stable slopes, as classified by Mandal and Maiti (2015), at the exception of already a dozen hotspots of steep slopes (see Figure 2b), where the $FOS \leq 1.0$

https://doi.org/10.5194/egusphere-2026-3426
Preprint. Discussion started: 29 June 2026

indicating instability. It demonstrates that topography and soil properties alone can predispose certain locations to failure even in the dry season and absence of earthquakes.

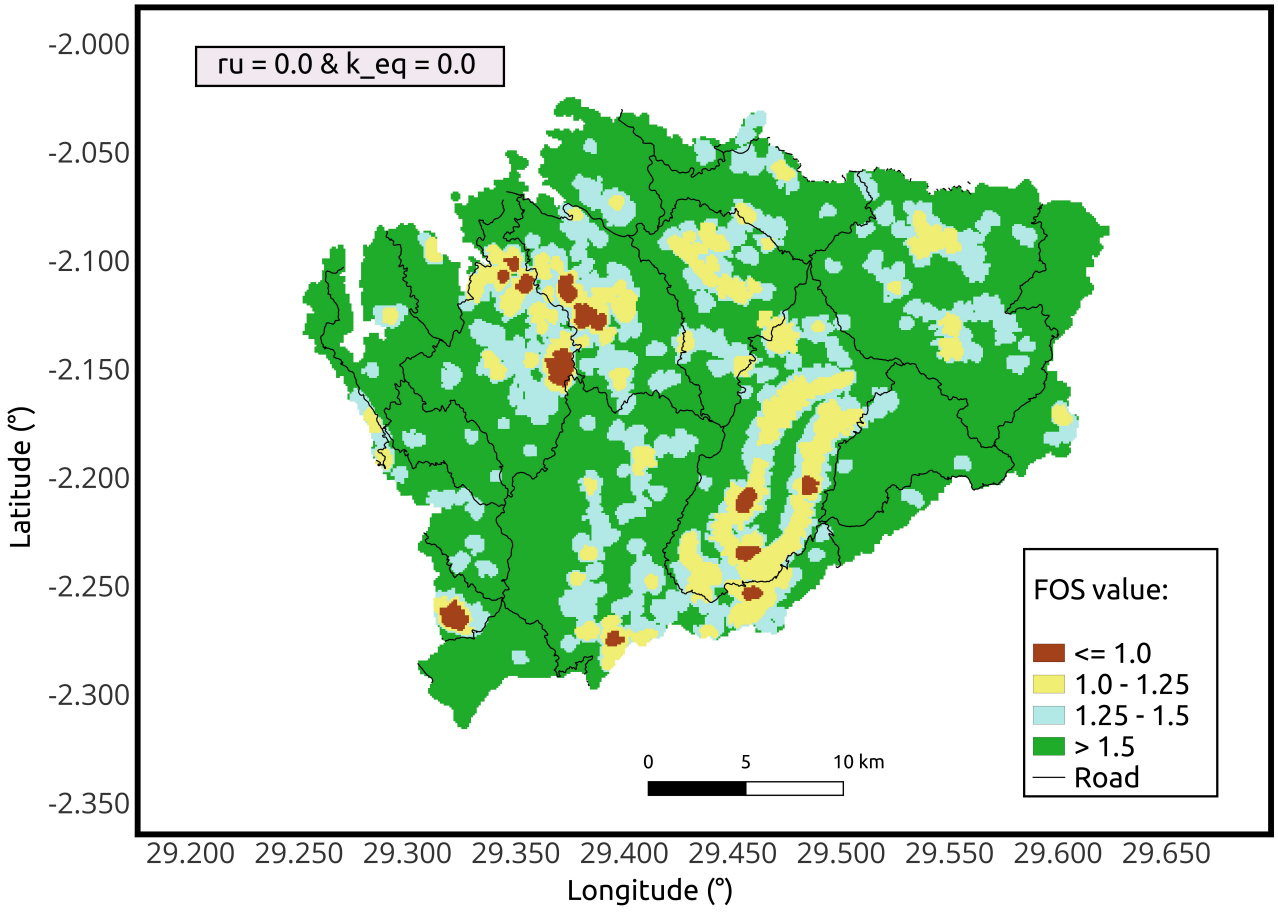

Figure 5. Baseline map of the FOS for $ru = 0.0$ and k_{eq} = 0.0, based on DEM and soil properties

https://doi.org/10.5194/egusphere-2026-3426
Preprint. Discussion started: 29 June 2026

4.2 Effect of increasing pore-pressure ratio

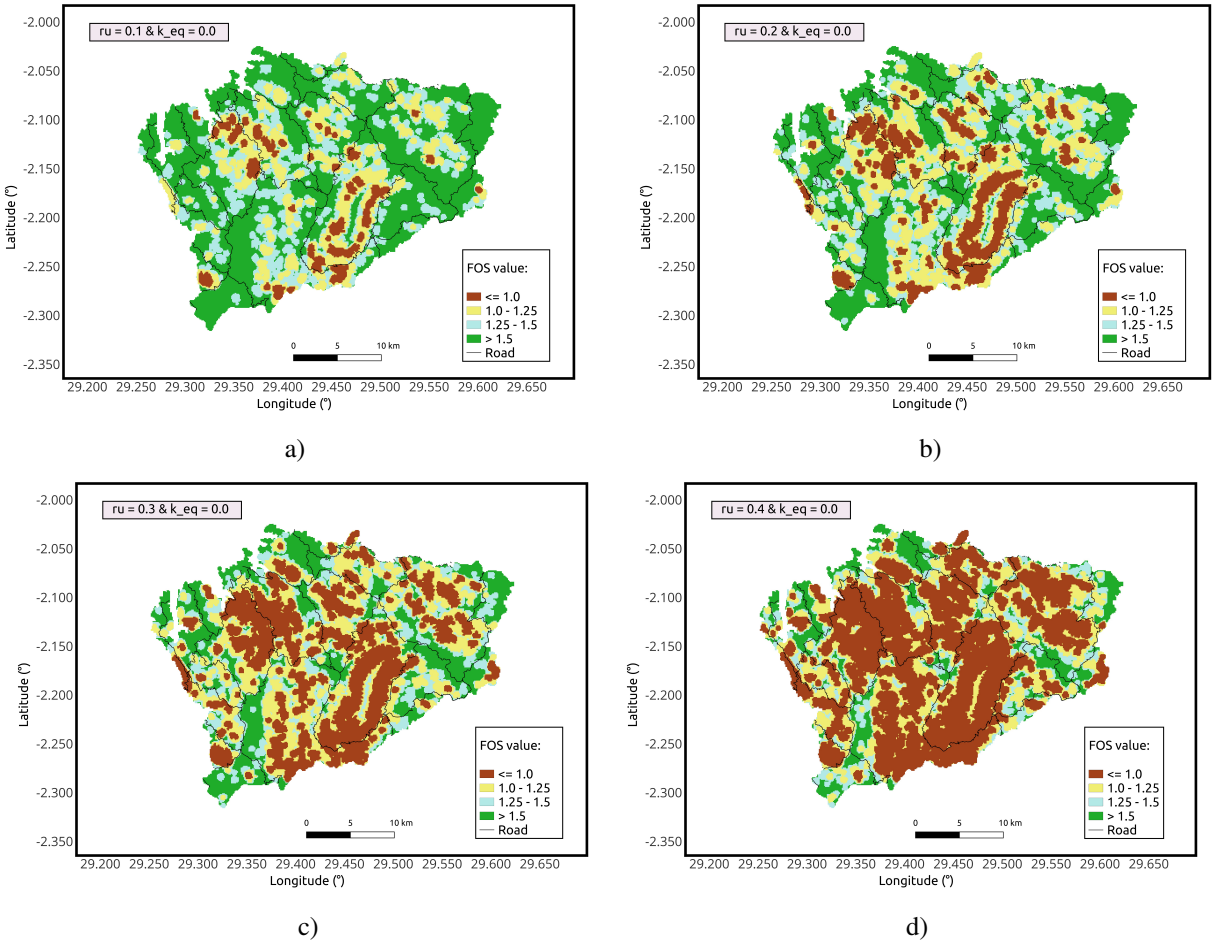

Figure 6. a) FOS maps as a function of pore-pressure ratio ru in absence of seismic loading ($k_{eq} = 0$). a) $ru = 0.1$. b) $ru = 0.2$ c)$ru = 0.3$. d) $ru = 0.4$

Figure 6 shows maps of the simulated FOS by increasing values of the pore-pressure ratio, ru. As expected, there is an increase in slope instability over the area of interest extending to medium slopes compared to Figure 5, but such increase appears to be moderate between $ru = 0$ and $ru = 0.15$ while it is more noticeable from $ru = 0.15$. At $ru = 0.4$, the extent of the areas where $FOS \leq 1$, appears to cover a very significant portion of the Karongi district, which is likely unrealistic.

Figure 7 further shows that the effect of ru on FOS is not identical or linear over the entire range of ru values. In particular, a sharp change in the influence of ru on the slope stability is observed as the pore-pressure ratio becomes greater than 0.15. From $0.15 \leq ru \leq 0.4$, the percentage of unstable areas with FOS less than one varies as a function of ru as $FOS_{\leq 1} = a\,ru^{1.678666}$, where $a = 251.5506$. For $ru > 0.4$, the FOS departs from the previous power law, suggesting that the Mohr-Coulomb criterion

https://doi.org/10.5194/egusphere-2026-3426
Preprint. Discussion started: 29 June 2026

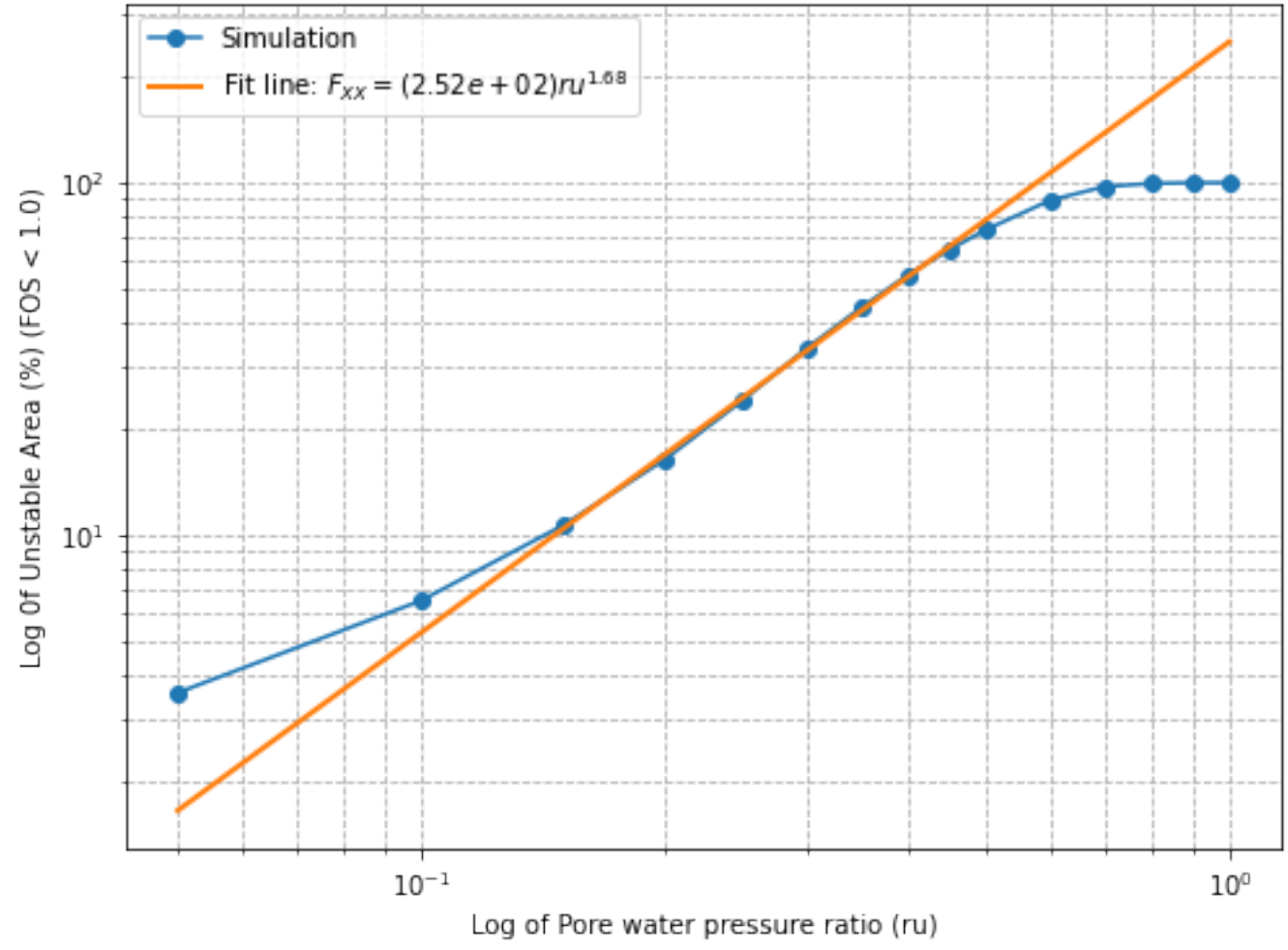

Figure 7. Percentage of unstable areas ($FOS < 1.0$) as a function of pore-pressure ratio (ru) under no seismic forcing with fit line

is likely no longer applicable and weakens the limit equilibrium assumptions. Figures 6 and 7 show that the increase of pore water pressure ratio alone can trigger substantial slope collapse.

4.3 Effect of seismic forcing

Figure 8 shows the spatial extent of the unstable simulated areas ($FOS_{\leq 1}$) in drained conditions for increasing values of k_{eq}.
180 The expected increase in unstable areas with the increase in seismic forcing highlights the same areas prone to landslides as those identified by the increase in pore-pressure along a direction northwest-southeast in central Karongi district. Similar to the influence of the pore-pressure ratio, such increase appears to be moderate between $k_{eq} = 0.03$ and $k_{eq} = 0.075$ while it is noticeable from $k_{eq} = 0.075$ (see Figure 9).

https://doi.org/10.5194/egusphere-2026-3426
Preprint. Discussion started: 29 June 2026

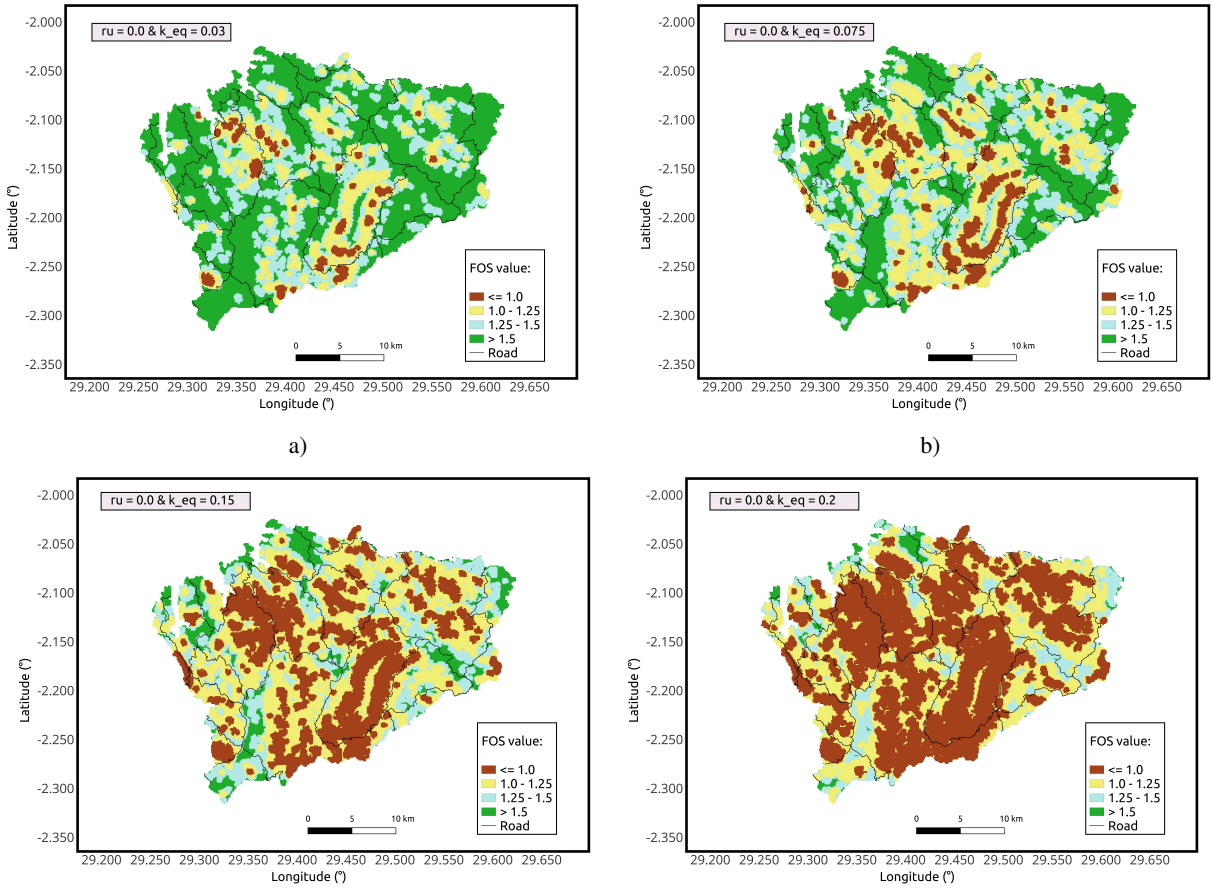

Figure 8. a) FOS maps as a function of horizontal pseudo-acceleration coefficient (fraction of g) a) $k_{eq} = 0.03$, b) $k_{eq} = 0.075$, c) $k_{eq} = 0.15$, and d) $k_{eq} = 0.2$ at pore-pressure ratio $ru = 0.0$

In parallel to Figure 7, the sole influence of the seismic forcing k_{eq} on the FOS in the absence of pore-pressure ($ru = 0$) is not identical or linear over the entire range of k_{eq} values as shown in Figure 9. In particular, a change in the impact of k_{eq} on the slope stability is observed as the horizontal pseudo acceleration becomes greater than 0.075-0.1. In the interval $0.075 - 0.1 \leq k_{eq} \leq 0.2$, the FOS varies as a function of k_{eq} as $FOS = b\,k_{eq}^{1.732302}$, where $b = 883.4671$. For $k_{eq} > 0.2$, the FOS departs from the previous power law. Compared to increasing the pore water pressure ratio, Figure 8 shows that quasi-stable areas (areas with $1.0 \geq FOS \leq 1.25$) is extending more rapidly than areas with $FOS < 1.0$ when k_{eq} increases.

4.4 Combined effect of pore-pressure and seismic forcing

Figure 10 shows the combined effect of pore-pressure and seismic forcing. While increasing pore-pressure, the amplification in the percentage of the unstable areas (Figure 10b), defined as the ratio between the % of unstable area for $k_{eq} \neq 0$ and $k_{eq} = 0.0$,

https://doi.org/10.5194/egusphere-2026-3426
Preprint. Discussion started: 29 June 2026

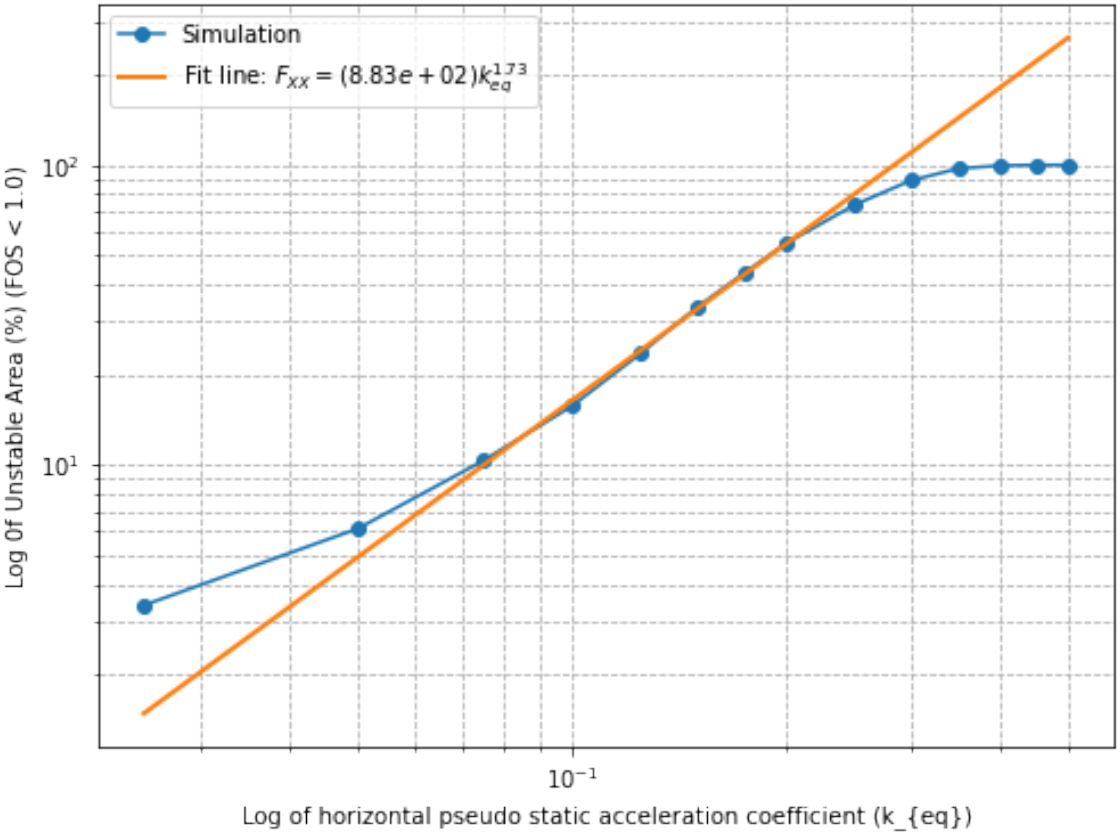

Figure 9. Percentage of unstable Area ($FOS < 1$) vs Horizontal pseudo-static acceleration coefficient (k_{eq}) at pore-pressure ratio $ru = 0.0$.

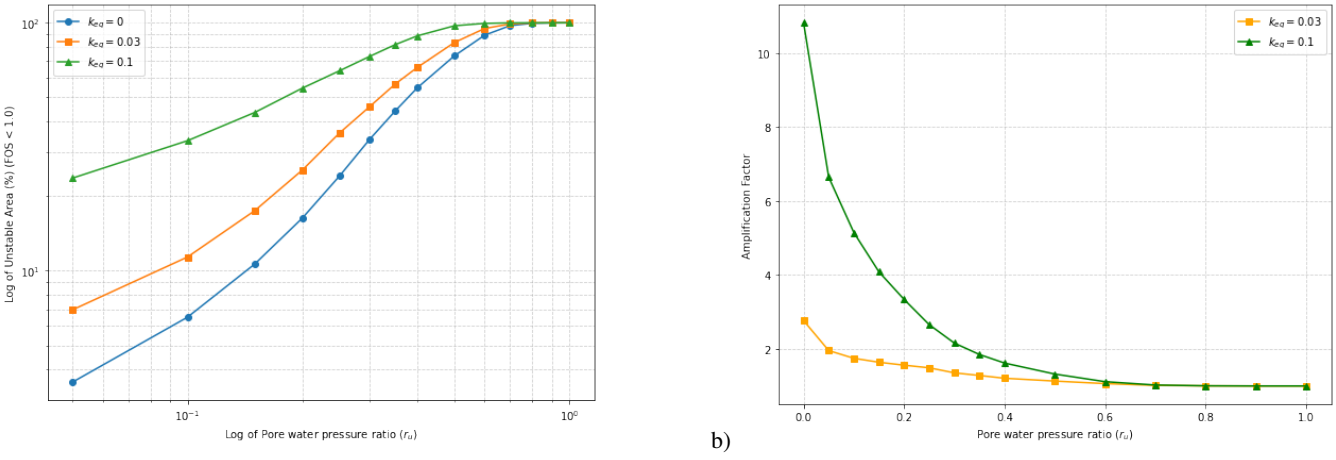

a) b)

Figure 10. a) The % unstable areas ($FOS_{\leq 1}$) as a function of ru for values of $k_{eq} = 0, 0.03$ & 0.1. b) Ratio of the $FOS_{\leq 1}|_{k_{eq} \neq 0}$ by the $FOS_{\leq 1}|_{k_{eq}=0}$

https://doi.org/10.5194/egusphere-2026-3426
Preprint. Discussion started: 29 June 2026

respectively, due to increasing seismic forcing is noticeable over all the range of pore-pressure ratios $ru \leq 0.6$, which is beyond the maximum of 0.4 as noted in section 4.2. In the range of low pore-pressure ratio ($ru \leq 0.1$), the seismic loading causes a maximum amplification of instability with a factor ranging from ~ 2 to 5 at $k_{eq} = 0.03$ and 0.1, respectively.

4.5 Comparison with historical landslide inventory

The FOS simulated results are compared with historical landslides catalog compiled by Depicker et al. (2021a) complemented with a landslide inventory built from visual inspection in Google Earth Pro. It should be noted that this inventory highlights landslides in the area of the south-east horseshoe-like pattern, which are completely absent from the catalog.

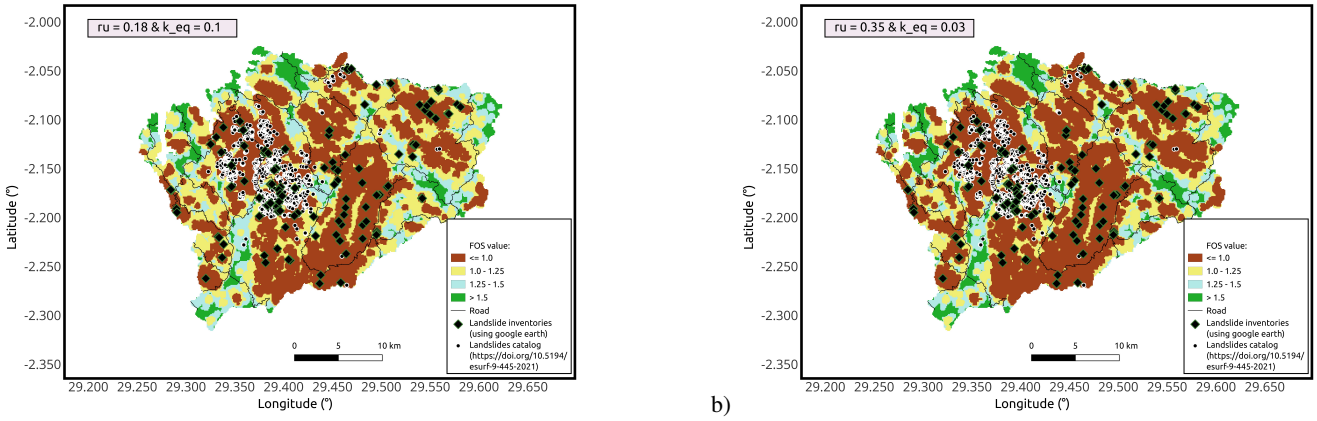

a) b)

Figure 11. Model validation using historical landslide inventories prepared by Depicker et al. (2021a) in complement with landslide inventories obtained using Google Earth pro overlapped on FOS map at a) $ru = 0.18$ with $k_{eq} = 0.1$, and b) $ru = 0.35$ with $k_{eq} = 0.03$

These landslides are overlapped on two FOS maps using $ru = 0.35$ with $k_{eq} = 0.03$ and $ru = 0.18$ with $k_{eq} = 0.1$, as shown in Figure 11, where about 80% historical landslides similarly align with the predicted unstable areas ($FOS < 1.0$). The observed correspondence between the model outputs and the landslide record distribution in the district validates the model's ability to inform on slope instability in the region. It also shows that there is not a single best fit solution.

5 Discussion and conclusion

Departing from susceptibility studies such as Malyse and Aboubakar (2025); Nsengiyumva et al. (2018), this paper reports on the first modelling study on landslides applied in Rwanda using the slope stability approach. We demonstrate that even in the context of a simplified approach, such modelling can be useful to identify potential areas of instability. This modelling could easily be extended to the Northern province, where numerous landslides have been reported and to the specific sites of interest at a higher resolution than this study. The analysis of the influence of unstable zones as a function of pore-pressure and seismic loading reveals three interesting behaviors: 1) The pore-pressure ratio has a moderate influence on the instability until $ru \sim 0.15$, 2) the influence of the seismic forcing on the slope stability is favored by a minimum horizontal pseudo

https://doi.org/10.5194/egusphere-2026-3426
Preprint. Discussion started: 29 June 2026

acceleration coefficient of $k_{eq} = 0.075$, and 3) the amplitude of the unstable zone increases at low pore-pressure ($ru \leq 0.1$) in the presence of seismic forcing, this increase being greater as the seismic forcing increases. Thus, we observe about five times more unstable zones for a horizontal pseudo-acceleration coefficient of $k_{eq} = 0.1$ compared to $k_{eq} = 0$ when $ru \leq 0,1$. With respect to Karongi district, an 80 % match between the simulated region for a $FOS \leq 1$ and the locations of historical landslides is observed, whether for a pore-pressure ratio $ru = 0.18$ and a seismic force $k_{eq} = 0.1$, or for a pore-pressure ratio $ru = 0.35$ and a negligible seismic force $k_{eq} = 0.03$. This suggests that pore-pressure in the Karongi district is an important factor contributing to landslides, but also that seismic load cannot be systematically neglected, since both a negligible seismic force and a larger seismic force ($k_{eq} = 0.03$ and 0.1) require pore-pressure ratios of 0.35 and 0.18, already indicative of a high degree of saturation (see for example Figure 3 of Mousavi and Ghayoomi (2020)). Compared to previous studies that emphasized rainfall-induced landslides in the Karongi district (Nwazelibe et al., 2023; Malyse and Aboubakar, 2025; Ngaboyigihugu et al., 2025) or that reported an exceptional landslide event, with approximately 700 landslides recorded in May 2018 and attributed to extreme weather conditions and not correlated with earthquakes (Byiringiro et al., 2024), this study shows that this phenomenon probably does not apply to all landslides and that seismic force could simply go unnoticed. In this respect, it is regrettable that the historical data available on landslide inventories (Depicker et al., 2021a) do not systematically provide the dates of the events, which could have revealed certain correlations (temporal and/or spatial) with those of the earthquakes.

Overall, two areas of the district appear susceptible to landslides: the northwest and the area marked by a horseshoe in the southeast, suggesting a northwest-southeast trend. At the periphery, two hotspots (northeast and southwest) in closer proximity to earthquakes as shown by Panelli et al. (2024) are also unstable. As the Karongi district extends towards Lake Kivu and given the bathymetry (Figure 1 of Kranenburg et al. (2020)), we should expect sub-aqueous landslides in the district (see Figure 6c & d or Figure 11). Compared to the Karongi district, the northern districts are characterized (apart from similarly steep slopes) by lower rainfall (see Figure 2d of Panelli et al. (2024)) and earthquakes with closer epicenters (See Figure 3), so we should also expect a greater impact of seismic forcing and less of pore-pressure with regard to slope stability in these districts. This study uses the Scoops3D software to map the factor of safety across a 3D digital elevation model (DEM). We modeled how pore pressure (r_u) and seismic loading (k_{eq}) affect slope stability, validating our approach with historical landslide inventories. We found that seismic activity significantly increases slope instability when pore water pressure is low. While this specific model targets the Karongi district in Rwanda, the workflow provides a universal methodology for evaluating unstable terrain in any seismically active region.

Appendix A: Influence of the DEM resolution on the FOS

Throughout this paper, we use a 100 m DEM and potential failure volumes of $10^7 - 10^8$ m^3 associated with the intrinsic Scoops3d parameters and options for the search lattice given in Table A1 to run the simulations.

https://doi.org/10.5194/egusphere-2026-3426
Preprint. Discussion started: 29 June 2026

Parameters/Options	Values	Units
Potential Volume failure $V_{min} - V_{max}$	$10^7 - 10^8$	m^3
Size tolerance tol	10^6	m^3
Search lattice horizontal resolution	100	m
Options coarse-to-fine multiplier	1	-
Minimum vertical extent	1500	m
Maximum vertical extent	4000	m
Search lattice vertical resolution	100	m
Search lattice radius increment dr	50	m
Minimum number of active columns	100	-

Table A1. Parameters and options of Scoops3d adopted throughout this paper to perform the simulations with the 100m DEM.

In Figure A1 - A3, we show the FOS maps for three simulations: 1) with the 100 m DEM and the coarse-to-fine horizontal resolution option of the search-lattice with a multiplier of 8, 2) with the 100 m DEM and the coarse-to-fine horizontal resolution option of the search-lattice with a multiplier of 1, and 3) with the 10 m DEM and the coarse-to-fine horizontal resolution option of the search-lattice with a multiplier of 8. The computationally most effective simulation corresponds to choice 1). The three simulations highlight the same area of high vulnerability to landslides. However, the extent of the areas where $FOS \leq 1$ show some differences with 0.40%, 1.45% and 1.75% for respectively simulations 1 to 3. Simulations run for choice 2) are consistent with simulations run for choice 3).

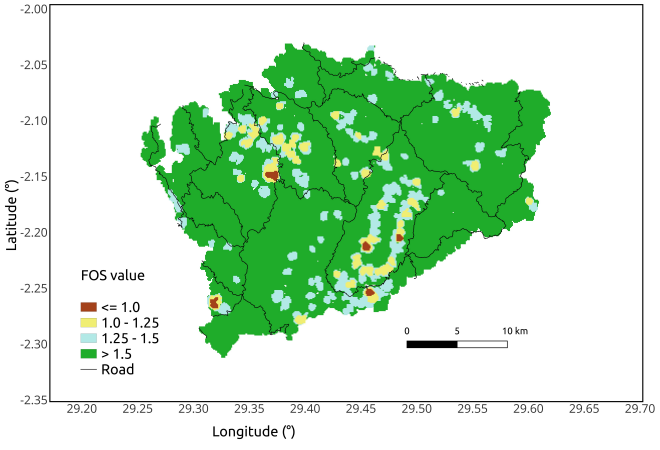

Figure A1. Map for DEM of 100 m resolution with a horizontal multiplier = 8, $ru = 0.0$, and $k_{eq} = 0.0$

https://doi.org/10.5194/egusphere-2026-3426
Preprint. Discussion started: 29 June 2026

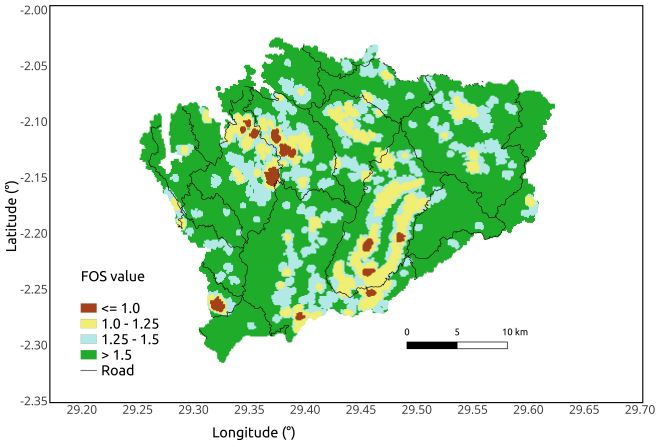

Figure A2. Map for DEM of 100 m resolution with a horizontal multiplier = 1, $ru = 0.0$, and $k_{eq} = 0.0$

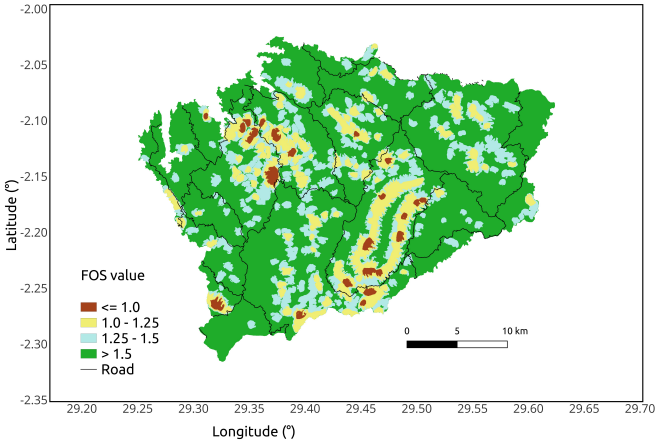

Figure A3. Map for DEM of 10 m resolution with a horizontal multiplier = 8, $ru = 0.0$, and $k_{eq} = 0.0$

Data availability. The data that support the findings of this study are publicly available:

Historical landslides inventories prepared by Depicker et al. (2021a) (https://zenodo.org/records/5027004),

Additional historical landslides inventories for Karongi district (Western Rwanda) derived from Google Earth Pro to complement the data inventories prepared by Depicker et al. (2021a) (https://doi.org/10.5281/zenodo.20736081),

Digital Elevation Model (DEM) with 10m resolution: https://geohub.data.undp.org/data/00d5add9be37e465398b081683c3ec03,

Used historical earthquakes near the study area (Karongi District) to calcurate Peak Ground Acceleration (PGA): https://doi.org/10.5281/zenodo.20736804 from (https://earthquake.usgs.gov/earthquakes/search/.)

https://doi.org/10.5194/egusphere-2026-3426
Preprint. Discussion started: 29 June 2026

Author contributions. SB, CM,and AA contributed to the study conception, design, material preparation, numerical modelling, analysis and validation; The first draft of the manuscript was written by SB and CM; AA reviewed and edited the manuscript.

Competing interests. The authors state that they have no known financial or personal conflicts of interest that could have influenced the research or findings presented in this paper.

Acknowledgements. This study has been supported by the Rwanda National Council for Science and Technology (NCST, project WALL, Grant ID: GCRW-CL001).

https://doi.org/10.5194/egusphere-2026-3426
Preprint. Discussion started: 29 June 2026

References

Bishop, A. W.: The Use of the Slip Circle in the Stability Analysis of Slopes, Geotechnique, 5, 7–17, https://doi.org/10.1680/geot.1955.5.1.7, 1955.

Bishop, A. W. and Morgenstern, N.: Stability Coefficients for Earth Slopes, Géotechnique, 10, https://doi.org/10.1680/geot.1960.10.4.129, 1960.

Byiringiro, F.V.and Jolivet, M., Dauteuil, O., Arvor, D., and Hitimana Niyotwambaza, C.: Exceptional Cluster of Simultaneous Shallow Landslides in Rwanda: Context, Triggering Factors, and Potential Warnings., GeoHazards, 5, 1018–1039, https://doi.org/10.3390/geohazards5040049, 2024.

Chowdhury, R. and Flentje, P.: Practical reliability approach to urban slope stability, Tech. rep., Faculty of Engineering, University of Wollongong, Wollongong, Australia, 2011.

Cruden, D. M. and Varnes, D. J.: Landslide Types and Processes, in: Special Report, 247, pp. 36–75, Transportation Research Board, U.S. National Academy of Sciences, 1996.

Depicker, A., Gerard, G., Liesbet, J., Benjamin, C., Judith, U., and Olivier, D.: Interactions between deforestation, landscape rejuvenation, and shallow landslides in the North Tanganyika–Kivu rift region, Africa, Earth Surface Dynamics, 9, 445–462, https://doi.org/10.5194/esurf-9-445-2021, 2021a.

Depicker, A., Jacobs, L., Mboga, N., Smets, B., Rompaey, A. V., Lennert, M., Wolff, E., Kervyn, F., Michellier, C., Dewitte, O., and Govers, G.: Historical dynamics of landslide risk from population and forest-cover changes in the Kivu Rift, nature sustainability, 4, 1–11, https://doi.org/10.1038/s41893-021-00757-9, 2021b.

Iverson, R. M.: Landslide triggering by rain infiltration, Water Resources Research, 36, 1897–1910, https://doi.org/10.1029/2000WR900090, 2000.

Kranenburg, W., Tiessen, M., Veenstra, J., de Graaff, R., Uittenbogaard, R., Bouffard, D., Sakindi, G., Umutoni, A., de Walle, J. V., Thiery, W., and v. Lipzig, N.: 3D-modelling of Lake Kivu: Horizontal and vertical flow and temperature structure under spatially variable atmospheric forcing, vol. 46, pp. 947—960, https://doi.org/10.1016/j.jglr.2020.05.012, 2020.

Malyse, M. and Aboubakar, G.: Geospatial Analysis of Landslide Susceptibility and Its Impact on Community Livelihood in Rwanda: A Case of Nyabihu District, International Journal of Advances in Engineering and Management, 7, 126–144, https://doi.org/10.35629/5252-0705126144, 2025.

Mandal, S. and Maiti, R.: Semi-Quantitative Approaches for Landslide Assessment and Prediction, Springer Natural Hazards, Springer, Singapore, https://doi.org/10.1007/978-981-287-146-6, 2015.

Mousavi, S. and Ghayoomi, M.: A semi-empirical model to predict excess pore pressure generation in partially saturated sand, vol. 195, pp. 1–6, https://doi.org/10.1051/e3sconf/202019502026, 2020.

Ngaboyigihugu, J. P., Aiping, T., Musengimana, A., and Mbarushimana, Y.: Soil Instability and Prevention Countermeasures of Typical Landslide in Northwest Rwanda, International Journal of Multidisciplinary Research and Analysis, 08, 4418–4428, https://doi.org/10.47191/ijmra/v8-i08-04, 2025.

NISR: The Fifth Rwanda Population and Housing Census, District Profile: Karongi, 2023.

Niyibizi, J. P., Bizimana, H., and Sobio, Y.: Slope Failure Analysis, Causes, and Sustainable Stabilization Measures: A Case Study of Rutsiro district, Rwanda, Brainae Journal of Business, Sciences and Technology., 9, 636–647, https://doi.org/10.5281/zenodo.15384413, 2025.

https://doi.org/10.5194/egusphere-2026-3426
Preprint. Discussion started: 29 June 2026

Nsengiyumva, Baptiste, J., Geping, L., Nahayo, L., Huang, X., and Peng, C.: Landslide Susceptibility Assessment Using Spatial Multi-Criteria Evaluation Model in Rwanda, International Journal of Environmental Research and Public Health, 7, 1–23, https://doi.org/10.3390/ijerph15020243, 2018.

Nwazelibe, V. E., Egbueri, J. C., Unigwe, C. O., Agbasi, J. C., Ayejoto, D. A., and Abba, S. I.: GIS-Based Landslide Susceptibility Mapping of Western Rwanda: An Integrated Artificial Neural Network, Frequency Ratio, and Shannon Entropy Approach, Environmental Earth Sciences, 82, 439, https://doi.org/10.1007/s12665-023-11134-4, 2023.

Osawa, H., Matsushi, Y., Matsuura, S., and Okamoto, T.: Semiempirical modeling of the transient response of pore pressure to rainfall and snowmelt in a dormant landslide, Landslides, 21, 245–256, https://doi.org/10.1007/s10346-023-02158-9, 2023.

Panelli, C., Vincenzo, M., Giorgio, P., Alberto, G., Paride, C., and Enrico, M.: Landslide susceptibility of Rwanda (Central Africa), Journal of Maps, 20, 1–12, https://doi.org/10.1080/17445647.2024.2428654, 2024.

Reid, M., Christian, S., Brien, D., and Henderson, S.: Scoops3D: Software to Analyze Three-dimensional Slope Stability Throughout a Digital Landscape, U.S. Geological Survey; Volcano Science Center, Menlo Park, https://doi.org/10.3133/tm14A1, 2015.

Schuster, R. L. and Highland, L. M.: Impact of Landslides and Innovative Landslide-Mitigation Measures on the Natural Environment, Tech. rep., Geologic Hazards Team, U.S. Geological Survey, Denver, Colorado, U.S.A., 2004.

Svalova, V. B., Zaalishvili, V. B., Ganapathy, G. P., Nikolaev, A. V., and Melkov, D. A.: Landslide Risk in Mountain Areas, Geology and Geophysics of the South of Russia, 10, 110–127, https://doi.org/10.23671/VNC.2019.2.31981, 2019.

Tuluka, M.: An estimate of the attenuation relationship for strong ground motion in the Kivu Province, Western Rift Valley of Africa, Physics of the Earth and Planetary Interiors, 162, 13–21, https://doi.org/10.1016/j.pepi.2007.02.001, 2007.